(4)

AD



TECHNICAL REPORT ARCCB-TR-88006

# THE GASDYNAMICS OF PERFORATED MUZZLE BRAKES

G. C. CAROFANO



FEBRUARY 1988

US ARMY ARMAMENT RESEARCH,
DEVELOPMENT AND ENGINEERING CENTER
CLOSE COMBAT ARMAMENTS CENTER
BENÉT LABORATORIES
WATERVLIET, N.Y. 12189-4050

## DISCLAIMER

The findings in this report are not to be construed as an official Department of the Army position unless so designated by other authorized documents.

The use of trade name(s) and/or manufacturer(s) does not constitute an official indorsement or approval.

## DESTRUCTION NOTICE

For classified documents, follow the procedures in DoD 5200.22-M, Industrial Security Manual, Section II-19 or DoD 5200.1-R, Information Security Program Regulation, Chapter IX.

For unclassified, limited documents, destroy by any method that will prevent disclosure of contents or reconstruction of the document.

For unclassified, unlimited documents, destroy when the report is no longer needed. Do not return it to the originator.

SECURITY CLASSIFICATION OF THIS PAGE *(When Data Entered)*

| REPORT DOCUMENTATION PAGE | | READ INSTRUCTIONS BEFORE COMPLETING FORM |
|---|---|---|
| 1. REPORT NUMBER<br>ARCCB-TR-88006 | 2. GOVT ACCESSION NO. | 3. RECIPIENT'S CATALOG NUMBER |
| 4. TITLE *(and Subtitle)*<br>THE GASDYNAMICS OF PERFORATED MUZZLE BRAKES | | 5. TYPE OF REPORT & PERIOD COVERED<br>Final<br>6. PERFORMING ORG. REPORT NUMBER |
| 7. AUTHOR*(s)*<br>G. C. Carofano | | 8. CONTRACT OR GRANT NUMBER*(s)* |
| 9. PERFORMING ORGANIZATION NAME AND ADDRESS<br>US Army ARDEC<br>Benet Laboratories, SMCAR-CCB-TL<br>Watervliet, NY 12189-4050 | | 10. PROGRAM ELEMENT, PROJECT, TASK AREA & WORK UNIT NUMBERS<br>AMCMS No. 6111.02.H610.000<br>PRON No. 1A7AZ703NMSC |
| 11. CONTROLLING OFFICE NAME AND ADDRESS<br>US Army ARDEC<br>Close Combat Armaments Center<br>Picatinny Arsenal, NJ 07806-5000 | | 12. REPORT DATE<br>February 1988<br>13. NUMBER OF PAGES<br>26 |
| 14. MONITORING AGENCY NAME & ADDRESS*(if different from Controlling Office)* | | 15. SECURITY CLASS. *(of this report)*<br>UNCLASSIFIED<br>15a. DECLASSIFICATION/DOWNGRADING SCHEDULE |

16. DISTRIBUTION STATEMENT *(of this Report)*

Approved for public release; distribution unlimited.

17. DISTRIBUTION STATEMENT *(of the abstract entered in Block 20, if different from Report)*

18. SUPPLEMENTARY NOTES

Presented at the Fifth U.S. Army Symposium on Gun Dynamics, The Institute on Man and Science, Rensselaerville, New York, 23-25 September 1987. Published in the Proceedings of the Symposium.

19. KEY WORDS *(Continue on reverse side if necessary and identify by block number)*

Perforated Muzzle Brake
Muzzle Brake
Muzzle Brake Efficiency
Weapon Impulse

20. ABSTRACT *(Continue on reverse side if necessary and identify by block number)*

In a study of perforated muzzle brakes, Nagamatsu, Choi, Duffy, and Carofano calculated the three-dimensional steady flow of a perfect gas through one vent hole and used the results to predict overall brake performance. The importance of the gas covolume is considered here by using the Abel equation of state.

(CONT'D ON REVERSE)

DD FORM 1 JAN 73 1473 EDITION OF 1 NOV 65 IS OBSOLETE

UNCLASSIFIED

SECURITY CLASSIFICATION OF THIS PAGE *(When Data Entered)*

20. ABSTRACT (CONT'D)

The brake performance calculations in the above study were limited to sets of holes of a single diameter. The merit of using sets of varying diameters is explored with particular emphasis on enhancing the structural integrity of the brake.

In studies of conventional muzzle brakes, the gasdynamic efficiency, $\beta$, has been found useful for comparing various brake designs and for scaling. A simple formula is presented which represents the efficiency of a wide variety of axisymmetric perforated brakes.

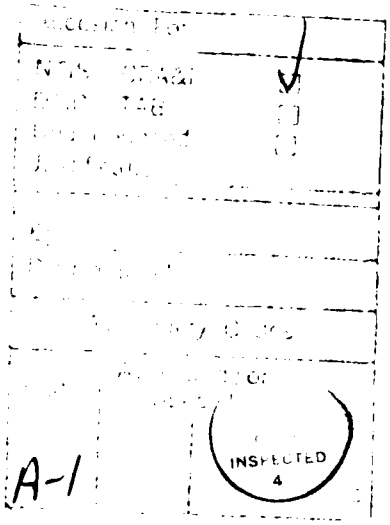

## TABLE OF CONTENTS



### TABLES



### LIST OF ILLUSTRATIONS

## INTRODUCTION

A perforated muzzle brake consists simply of a set of vent holes drilled through the wall of a cannon near the muzzle (see Figure 1). Compared with conventional baffle brakes, they are lighter and simpler to manufacture and, as shown in a series of reports by Dillon and Nagamatsu (refs 1-5), they can be designed to provide significant levels of recoil reduction. Also, because the vented area can be located symmetrically around the tube, a more favorable flow environment is provided for finned projectiles. This is an important consideration for weapon accuracy and the structural integrity of the projectile. In a field study of 105-mm brake designs, it was found that asymmetrical venting can lead to bending and even breakage of the fins.

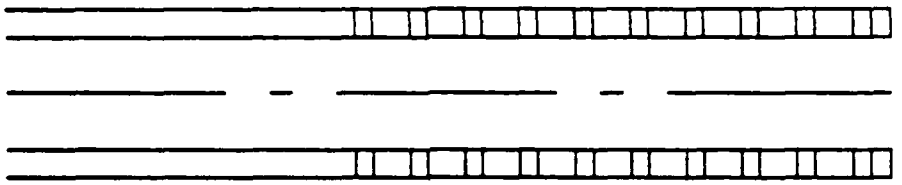

Figure 1. Schematic drawing of a perforated muzzle brake.

Nagamatsu, Duffy, Choi, and Carofano (ref 6) made a numerical calculation of the steady three-dimensional flow through a vent hole in the wall of a shock tube. The predicted pressure distribution on the vent wall compared favorably with the experimental measurements of Nagamatsu, Duffy, and Choi (ref 7). It was also shown that these results could be combined with a one-dimensional model of the transient flow in a cannon to predict the impulse reduction produced by a perforated muzzle brake. The predictions agreed well with the experimental measurements of Dillon (ref 1) for a 20-mm cannon.

---

References are listed at the end of this report.

These calculations were made for a perfect gas, but at the pressure levels found in larger caliber weapons, the necessity of including the gas covolume correction in internal ballistics solutions is well known (ref 8). The importance of this factor on perforated muzzle brake performance is considered here.

It is also of interest to know if and how experimental results obtained with a small caliber weapon can be scaled up in an effort to avoid the high costs associated with testing larger weapons. In studies of conventional muzzle brakes (refs 9-11), the gasdynamic efficiency, $\beta$, has been found useful for this purpose. Its application to perforated muzzle brakes is discussed here.

## THE THREE-DIMENSIONAL MODEL

When the propellant gas expands through the brake, an asymmetric pressure distribution develops in each hole with the highest pressures acting on the downstream surface. The vector and pressure contour plots of Figures 2 and 3 show typical flow patterns in the symmetry plane of one hole and the portion of the tube associated with it. The flow variables in the tube are uniform across the entrance plane. The solid lines in the vector plot indicate where the local Mach number is unity.

In Figure 2, the flow enters at Mach one and accelerates to supersonic velocities as a portion of the gas expands and turns into the hole. The shock at the downstream lip of the hole turns the expanded flow parallel to the solid surfaces and reduces the velocities to subsonic levels. The pressure on the lip is nearly twice the static pressure of the incoming stream. The flow accelerates away from this region and leaves the tube and hole at supersonic velocities. There is a large subsonic region on the upstream portion of the hole where the pressure is nearly uniform. A more complete description of the three-

dimensional flow pattern, as well as a comparison with experimental data, is given in Reference 6.

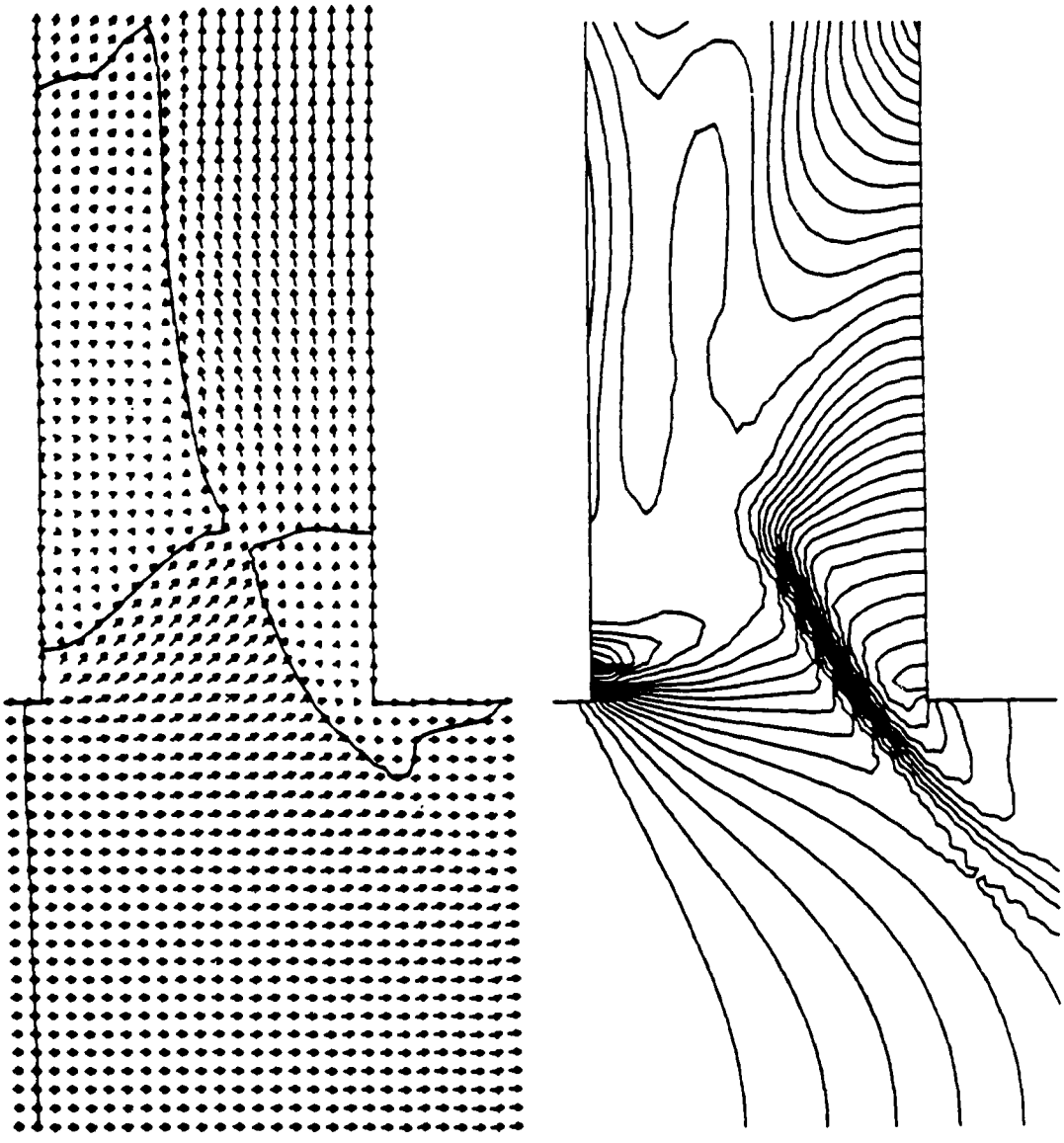

Figure 2. Velocity vector and pressure contour plots for a flow with a Mach number of unity at the entrance plane.

To calculate the resulting braking force, a detailed knowledge of the pressure distribution acting on all surfaces of the brake is required at each instant of time during tube blowdown. Because the flow is three-dimensional, it is not practical to obtain the complete solution with one numerical calculation.

Fortunately, the flow contains many features which permit a vigorous simplification of the problem.

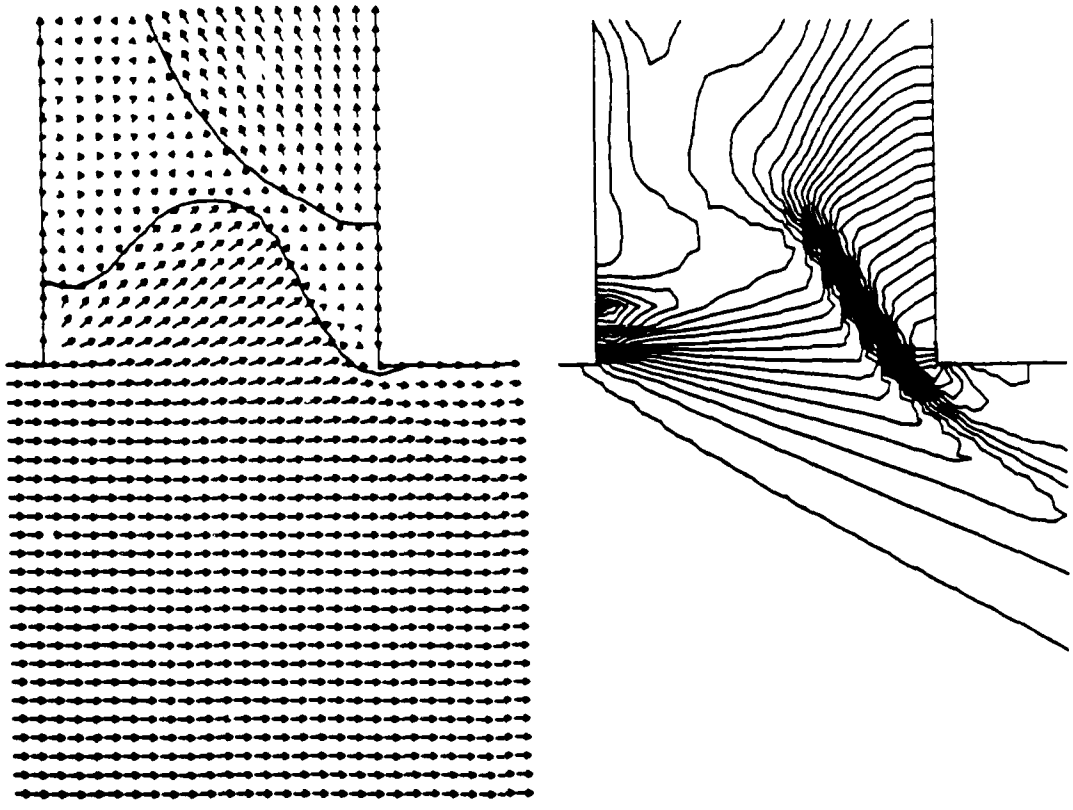

Figure 3. Velocity vector and pressure contour plots for a flow with a Mach number of two at the entrance plane.

First, because of the large volume of the gun tube, the blowdown process takes on the order of tens of milliseconds while the three-dimensional calculations indicate that the flow in a hole is established in a fraction of a millisecond. Therefore, the latter can be treated as quasi-steady and only the flow within the tube must be considered as a time-dependent process.

Secondly, in the applications of interest, the flow is either sonic or supersonic as it enters the brake and, due to the venting, expands to higher Mach numbers as it travels downstream. Also, because of the high tube

pressures, the gas exits each hole near sonic or supersonic velocity over most of the exit plane area (see Figures 2 and 3). Experience has shown that the flow is rather insensitive to the outflow boundary condition over the remaining subsonic portion. Thus, the flow at a particular hole location is not influenced by events occurring farther downstream or outside of the tube. It depends solely on the conditions in the tube upstream of the hole. This observation permits a dramatic reduction in the amount of three-dimensional computation required to predict brake performance.

The Euler equations may be written in conservative form as

$$\frac{\partial Q}{\partial t} + \frac{\partial F}{\partial x} + \frac{\partial G}{\partial y} + \frac{\partial H}{\partial z} = 0 \qquad (1)$$

where

$$Q = \begin{bmatrix} \rho \\ m \\ n \\ \ell \\ E \end{bmatrix}, \quad F = \begin{bmatrix} m \\ m^2/\rho+P \\ mn/\rho \\ m\ell/\rho \\ (E+P)m/\rho \end{bmatrix}, \quad G = \begin{bmatrix} n \\ nm/\rho \\ n^2/\rho+P \\ n\ell/\rho \\ (E+P)n/\rho \end{bmatrix}, \quad H = \begin{bmatrix} \ell \\ \ell m/\rho \\ \ell n/\rho \\ \ell^2/\rho+P \\ (E+P)\ell/\rho \end{bmatrix}$$

$\rho$ is the density; $m = \rho u$, $n = \rho v$, and $\ell = \rho w$ are the momentum components in the x, y and z directions, respectively; u, v, and w are the corresponding velocity components. P is the pressure and E is the total energy per unit volume defined as

$$E = \rho e + (m^2+n^2+\ell^2)/2\rho \qquad (2)$$

where e is the specific internal energy.

To include the influence of the gas covolume, $\eta$, the Abel equation of state is used. For this model, the pressure and soundspeed, c, are related to the state variables $\rho$ and e by the expressions

$$P = (\gamma-1)\rho e/(1-\eta\rho) \tag{3}$$

$$c^2 = \gamma(\gamma-1)e/(1-\eta\rho)^2 \tag{4}$$

where $\gamma$ is the specific heat ratio.

Consider the result of nondimensionalizing the Euler equations in the following way:

$$\rho' = \rho/\rho_2 \quad , \quad m' = m/\sqrt{P_2\rho_2} \quad , \quad n' = n/\sqrt{P_2\rho_2} \quad , \quad \ell' = \ell/\sqrt{P_2\rho_2}$$

$$P' = P/P_2 \quad , \quad E' = E/P_2 \quad , \quad e' = e\rho_2/P_2 \quad , \quad c' = c\sqrt{\rho_2/P_2}$$

$$x' = x/D \quad , \quad y' = y/D \quad , \quad z' = z/D \quad , \quad t' = t\sqrt{P_2/\rho_2}/D$$

where $\rho_2$ and $P_2$ are the density and pressure of the uniform flow at the upstream plane of the tube and D is the vent diameter. The form of the Euler equations remains unchanged while the inflow boundary conditions become

$$\rho' = 1 \tag{5}$$

$$m' = M_2\sqrt{\gamma/(1-\eta\rho_2)} \tag{6}$$

$$n' = \ell' = 0 \tag{7}$$

$$E' = (1-\eta\rho_2)/(1-\gamma) + \gamma M_2^2/2(1-\eta\rho_2) \tag{8}$$

The pressure and soundspeed relations become

$$P' = (\gamma-1)\rho' e'/(1-\eta\rho_2\rho') \tag{9}$$

$$c'^2 = \gamma(\gamma-1)e'/(1-\eta\rho_2\rho')^2 \tag{10}$$

Since the flow depends only on the inflow boundary conditions, which are seen to be completely described by the upstream Mach number, $M_2$, the specific heat ratio, $\gamma$, and the dimensionless product, $\eta\rho_2$, one solution with these parameters specified is valid for all upstream pressures and densities. Although a wide range of physical states is encountered during blowdown, it is found that only a few three-dimensional solutions are required to describe them.

Harten's Total Variation Diminishing scheme (ref 12) was used in conjunction with a time-splitting algorithm to solve the Euler equations after they

were transformed to a generalized grid. Separate grids were used for the vent and the tube. A cylindrical grid was used for the vent with a Cartesian grid at its center to avoid the geometrical singularity there. The circular tube was replaced with a rectangular channel to simplify interpolation between the two grids. As can be seen in the vector plot of Figure 2, 19 grid points were used across the vent diameter and for the azimuthal coordinate. The length of the rectangular channel (the primary flow direction) was represented with 28 grid points, its height by 24 points, and its depth (into the paper) by 13 points.

Of course, the size of the channel could affect the flow through the vent. To check this possibility, the example shown in Figure 2 was repeated with the number of grid points used to represent the height and depth of the channel approximately doubled. The effect on the solution in the vent was minimal, indicating that the channel was essentially an infinite reservoir. The inflow Mach number in this example was unity. At Mach two, the effect would be expected to be even less because the disturbance produced by the vent occupies much less of the channel (see Figure 3).

## THE ONE-DIMENSIONAL MODEL

The one-dimensional equations of motion with venting at the tube wall are

$$\frac{\partial \rho}{\partial t} + \frac{\partial m}{\partial x} = \frac{1}{A}\frac{\dot{dm}}{dx} \tag{11}$$

$$\frac{\partial m}{\partial t} + \frac{\partial (m^2/\rho + P)}{\partial x} = \frac{m}{\rho A}\frac{\dot{dm}}{dx} \tag{12}$$

$$\frac{\partial E}{\partial t} + \frac{\partial (m(E+P)/\rho)}{\partial x} = \frac{(E+P)}{\rho A}\frac{\dot{dm}}{dx} \tag{13}$$

The vent term $(1/A)\dot{dm}/dx$ represents the mass of fluid per unit time per unit volume leaving the tube at x. A is the bore area. The fluid is assumed to leave at the local velocity u in the momentum equation and with the local enthalpy per unit mass $(E+P)/\rho$ in the energy equation (see Reference 13 for the derivation of these equations).

Data from the three-dimensional solution are used to obtain an average value for the dimensionless mass flux leaving the vent using the expression

$$\overline{\rho'w'} = (1/A_H)\int_{A_H}\rho'w'dA \qquad (14)$$

where w' is the dimensionless velocity in the z-direction, i.e., parallel to the vent axis. The integration is carried out over the vent exit area, $A_H$. The flux is applied instantaneously at each axial location in the one-dimensional model. It is a function of the three parameters that appear in the three-dimensional solution.

The mass flux also depends on the aspect ratio of the hole, which is defined as the ratio of its height, L, to its diameter, D. In Reference 6, the brake configurations were limited to sets of uniform diameter holes. However, from the structural point of view, it may be advantageous to use progressively smaller holes away from the muzzle, since the web of material between each successive row of holes must support the full load generated by all of the holes farther downstream. To allow for this possibility, the hole diameter will be taken as the following function of distance, y, along the brake:

$$D = D_{min} + (D_{max}-D_{min})(y/L_V)^a, \quad 0 < a < 1 \ , \ 0 < y < L_V \qquad (15)$$

where $L_V$ is the length of the vented region, $D_{min}$ is the diameter of the first row of holes at the brake entrance, and $D_{max}$ is the diameter of the last row of holes near the muzzle. Let $N_R$ be the number of rows of holes (rows run around

the circumference of the tube) and $N_C$ be the number of columns of holes (columns run parallel to the tube axis). For a uniform spacing of the holes along the brake, the vent area per unit length is $N_C N_R \pi D^2/4L_V$ and the total vent area, $A_V$, is found by integration to be

$$A_V = (\pi N_C N_R D_{min}^2/4)(1+2r/(a+1) + r^2/(2a+1)) \quad (16)$$

where r is the ratio

$$r = (D_{max}-D_{min})/D_{min} \quad (17)$$

The vent term can be written in dimensional form as

$$(1/A)\dot{dm}/dx = \overline{-\rho'w'}\sqrt{P\rho}\ (N_C N_R/L_V)(D/D_b)^2 \quad (18)$$

where $D_b$ is the tube diameter. P and $\rho$ are the local values of pressure and density in the one-dimensional solution; they appear since these quantities were used to nondimensionalize the product $\rho'w'$ in the three-dimensional solution.

Using a control volume drawn around the outer boundaries of the tube, including the muzzle exit plane, the following equation for the impulse, I, is obtained:

$$I = WV_{pe} + A\int_0^\infty (P_e-P_o+\rho_e u_e^2)dt + A\int_0^\infty [N_C N_R/L_V)\int_0^{L_V} \overline{\rho'w'u'}\ P(D/D_b)^2 dy]dt \quad (19)$$

The first term is the projectile momentum as it passes the brake exit plane with velocity $V_{pe}$. The second term is the thrust produced by the gas discharged through this plane. The subscript "e" refers to time-dependent properties obtained from the one-dimensional solution. $P_0$ is atmospheric pressure.

The quantity in brackets in the third term represents the axial thrust produced by the gas venting through the holes. As can be seen from the vector plots in Figures 2 and 3, the gas velocity is not, in general, parallel to the hole axis everywhere across the exit plane, so this integral may be negative, zero, or even positive. The average value of the momentum flux is calculated from the three-dimensional solution using the expression

$$\overline{\rho'w'u'} = (1/A_H)\int_{A_H}\rho'w'u'dA \tag{20}$$

where u' is the dimensionless axial velocity component of the vented gas. This quantity is a function of the local Mach number and geometry, just as with the mass flux. The local values of pressure and hole diameter appear in the spatial integral in Eq. (19) because they are position-dependent. The integral is evaluated at each time-step in the one-dimensional solution.

The calculation is started with the projectile base just upstream of the vented region. Initial conditions are taken from an internal ballistics code which uses the Pidduck-Kent limiting solution (ref 8) to compute the gradients of pressure, density, and velocity. These are given by

$$\Omega = \frac{(\gamma-1)}{2\gamma}\frac{C}{W}\left(\frac{(\gamma-1)}{2\gamma}\frac{C}{W} + \int_0^1 \left(\frac{1-\Omega\mu^2}{1-\Omega}\right)^{1/(\gamma-1)}d\mu\right)^{-1} \tag{21}$$

$$X = x/x_S \tag{22}$$

$$X = Z - \eta\frac{C}{U}\left(Z - \int_0^Z \left(\frac{1-\Omega\mu^2}{1-\Omega}\right)^{1/(\gamma-1)}d\mu \Big/ \int_0^1 \left(\frac{1-\Omega\mu^2}{1-\Omega}\right)^{1/(\gamma-1)}d\mu\right) \tag{23}$$

$$P = P_V\left(\frac{1-\Omega}{1-\Omega Z^2}\right)^{-\gamma/(\gamma-1)} \tag{24}$$

$$\frac{1}{\rho} - \eta = \left(\frac{U}{C} - \eta\right)\frac{(\gamma-1)}{2\gamma}\frac{(1-\Omega)}{\Omega}\frac{C}{W}\left(\frac{1-\Omega}{1-\Omega Z^2}\right)^{1/(\gamma-1)} \tag{25}$$

$$u = ZV_{PV} \tag{26}$$

where $P_V$ is the projectile base pressure at the starting time, $t_S$, and $V_{PV}$ is the projectile velocity. C and W are the charge and projectile masses, respectively. $\Omega$ is a parameter which depends on the ratio C/W and $\gamma$. It is evaluated once at the start of the solution by solving Eq. (21) by iteration. $x_S$ is the projectile position at time $t_S$; it includes a uniform extension of the tube of length U/A where U is the chamber volume and A is the bore area.

At each grid point in the one-dimensional solution, X is computed, then Z is found by iteration from Eq. (23). The values of pressure, density, and velocity are then calculated and the conservative variables in the Euler equations are formed from these.

The equation of motion for the projectile is solved together with the conservation equations until the projectile exits the barrel. The effect of brake venting on the final projectile velocity is thus determined. The remainder of the calculation deals with the motion of the gas in the barrel until complete blowdown is achieved.

## THE DIMENSIONLESS FLUX FUNCTIONS

Four factors affect the values of the dimensionless flux functions: the specific heat ratio, $\gamma$; the covolume parameter, $\eta\rho_2$; the upstream Mach number, $M_2$; and the vent geometry. $\gamma$ does not vary much for different propellants and its effect on the three-dimensional solution has been found through experience to be small. A single value of $\gamma = 1.22$ was used here to reduce the amount of calculation.

A study of internal ballistics solutions for various caliber weapons showed that the covolume parameter is not likely to exceed 0.2, therefore, this study used only this value and the perfect gas limit, $\eta\rho_2 = 0.0$.

In an earlier study (ref 6), the flux functions were found to vary nearly linearly with $M_2$, therefore, the calculations were limited to the two cases $M_2 = 1$ and $M_2 = 2$.

The hole geometry is characterized by the ratio of its height, L, to its diameter, D. The height is equal to the tube wall thickness which, in most designs, would be uniform throughout the brake. Manufacturing considerations suggest a range of L/D from 1 to 2 so these two values were used here.

These parameter choices required a total of eight three-dimensional solutions. The averaged flux functions are shown in Figure 4.

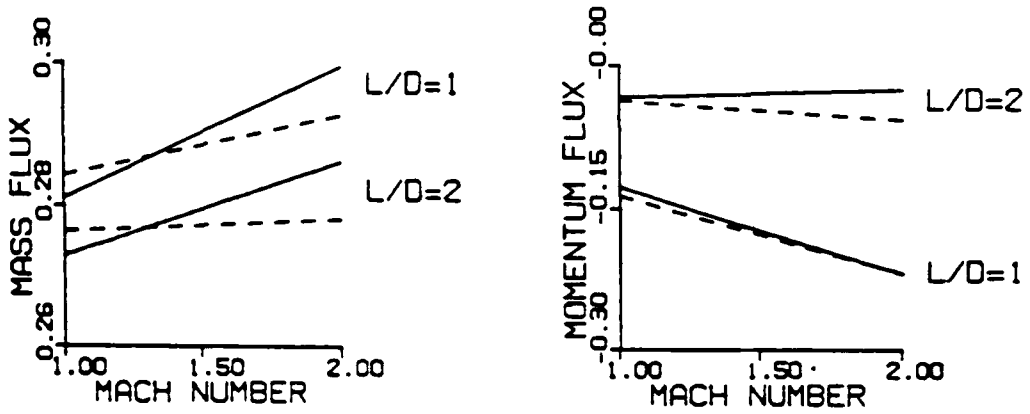


Figure 4. Averaged mass and momentum flux functions computed from the three-dimensional solutions.

The dashed lines represent the effect of including the covolume term in the equation of state. Since the covolume parameter was chosen to represent an upper limit of conditions expected in a brake, it would not appear to be very important. This was confirmed with several test cases using the one-dimensional code. It can be concluded that in any future three-dimensional studies, the effect of covolume on the flux functions and brake performance is too small to warrant doubling the amount of computation. The covolume term should be included in the equation of state used in the one-dimensional code, however, to be consistent with the internal ballistics code used to generate the starting solution.

Note that the momentum flux is negative for both vent heights, especially the shorter one. This is consistent with the velocity vector plots of Figures 2 and 3 -- the flow leaving the shorter vent is, on balance, directed more upstream.

The linear functions shown in Figure 4 were incorporated into the one-dimensional code as simple analytical expressions. Interpolation was used wherever necessary. The covolume correction was included since the information had already been obtained.

## BRAKE PERFORMANCE VERSUS VENT AREA DISTRIBUTION

Previous work (refs 1-6) has shown that when a brake is made with a set of uniform diameter holes, the hole diameter, D, should be set equal to the tube wall thickness, L, to achieve the greatest reduction in weapon impulse for a given vented area. This is a result of the asymmetrical pressure distribution in the hole. With reference to Figure 2, as the gas expands to supersonic velocities along the downstream wall, the gas pressure falls below the level acting on the adjacent upstream surface. The crossover occurs at a distance into the hole of about one diameter. Beyond this point the net braking load decreases. Thus, the most efficient brake is a set of uniform holes with L/D = 1. However, a less efficient brake might be preferred or even required based on structural considerations. This will be demonstrated using a 120-mm cannon as an example. The values in Table I were used to start the solution. $L_b$ is the barrel length, i.e., the total distance traveled by the projectile base. The other symbols were defined earlier.

Finned projectiles generally have six fins. To reduce asymmetrical loading of the fins as the projectile passes through the vented region and to limit circumferential pressure gradients, brakes are usually designed with twelve columns of holes so $N_C = 12$ will be used in all of the calculations below. The number of rows of holes, $N_R$, will be varied to obtain the vent area desired.

TABLE I. STARTING SOLUTION DATA

| Parameter | 120-mm Cannon | 20-mm Cannon |
|---|---|---|
| $P_v$ ($lb_f/in.^2$) | 12604.0 | 4219.0 |
| C ($lb_m$) | 19.59 | 0.0878 |
| W ($lb_m$) | 15.60 | 0.2161 |
| U ($in.^3$) | 595.0 | 2.545 |
| $V_{pv}$ (ft/sec) | 5073.6 | 3429.0 |
| $\gamma$ | 1.22 | 1.25 |
| $\eta$ ($in.^3/lb_m$) | 27.2 | 30.0 |
| $D_b$ (in.) | 4.724 | 0.7874 |
| $x_s$ (in.) | 170.9 | 56.3 |
| $L_b$ (in.) | 198.0 | 63.7 |
| L (in.) | 0.945 | 0.1575 |

Consider the two hole patterns in Figure 5 where three of the twelve columns of each brake are shown; the flow is from left to right. The uniform pattern has $D_{min} = D_{max} = L = 0.945$ inch for maximum efficiency; to maintain the same vent area, the stepped pattern used $D_{min} = 0.563$ inch, $D_{max} = 1.0$ inch, and $a = 0.6$ in the power law expression, Eq. (15). As indicated by the data above the patterns, redistributing the area in this manner increases the recoil impulse by less than two percent. However, because the total brake load is supported by a larger web area in the stepped design, the maximum axial load per unit web area is reduced by 40 percent (the maximum occurs at the instant the projectile base is at the muzzle). The variation of axial load per unit web area with distance along the brake is shown in Figure 6. The reduced stress levels near the brake entrance should have a favorable effect on fatigue life.

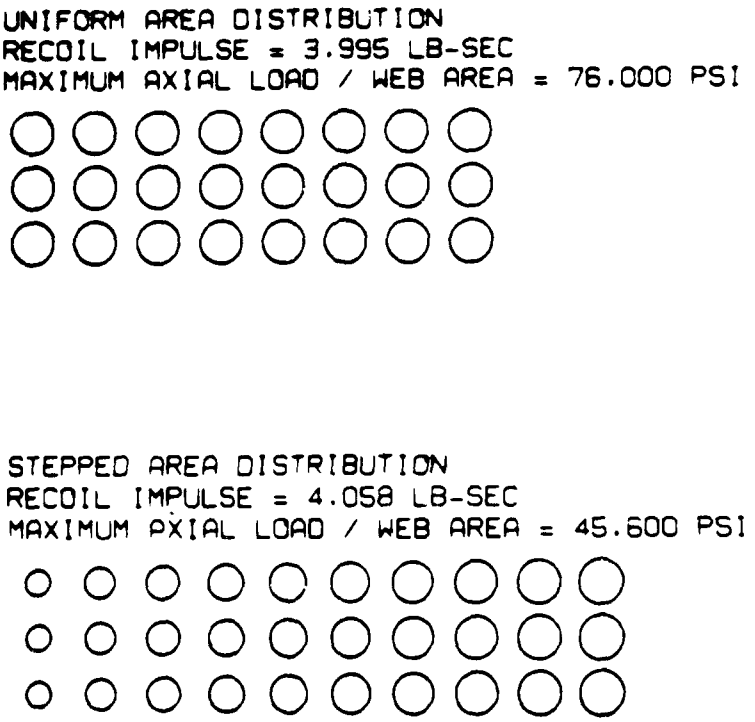


Figure 5. A comparison of a uniform hole pattern with a stepped pattern.

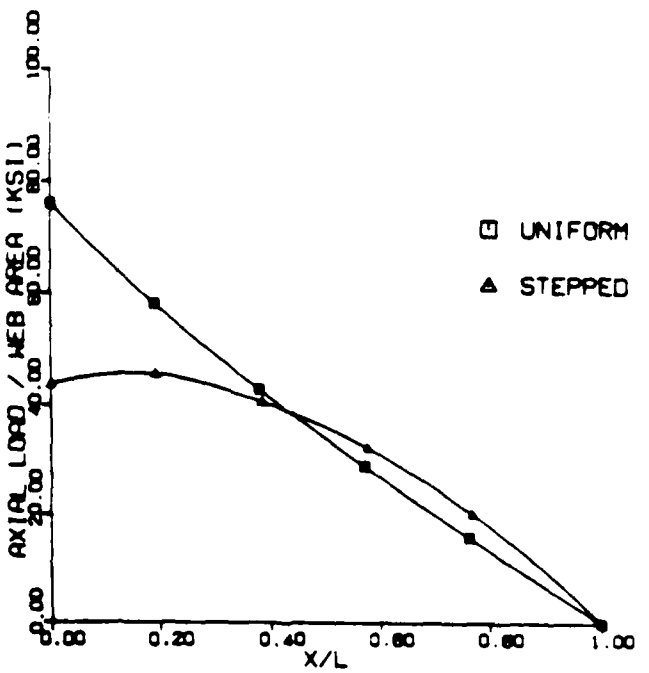


Figure 6. Axial load per unit web area along the brakes for the two patterns shown in Figure 5.

Because of the more gradual increase in vent area with distance in the stepped design, the drop in propellant gas pressure is more moderate, as shown in Figure 7. This implies that the pressure gradient in the azimuthal direction will also be smaller so a finned projectile will be exposed to a less severe loading as it passes through the brake.

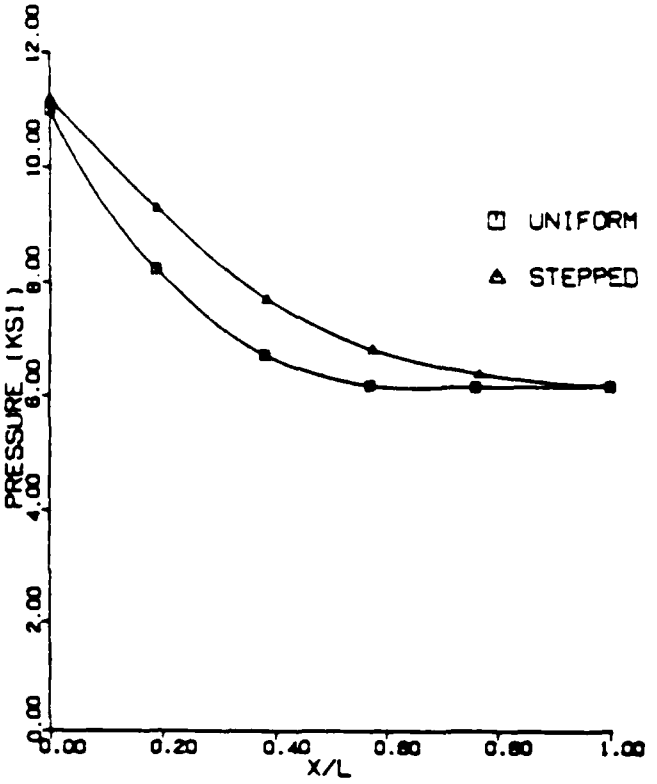


Figure 7. Pressure distribution along the brakes for the two patterns shown in Figure 5.

This example demonstrates that redistributing a given vent area along the tube can result in a structurally more acceptable design with only a modest loss in gasdynamic performance. In practice, of course, the stepped pattern would consist of a few different hole sizes rather than continuously varying diameters.

## BRAKE EFFICIENCY AND SCALING

A parameter that is useful for comparing the performance of conventional muzzle brakes is the gasdynamic brake efficiency, $\beta$, defined as

$$\beta = (I_{WO} - I_W)/(I_{WO} - WV_{PWO}) \tag{27}$$

where $I_W$ is the recoil impulse, W is the projectile mass and $V_P$ is its muzzle velocity. The subscript "wo" refers to the bare muzzle case.

$\beta$ is often found to be remarkably insensitive to the weapon caliber and internal ballistics and dependent only upon brake geometry. It is a practical tool for comparing various brake designs on a given weapon or for estimating performance based upon data obtained with a different caliber weapon. It will be demonstrated that this utility carries over to perforated muzzle brakes by comparing the performance of geometrically similar brakes on a 120-mm cannon and a 20-mm cannon. The data in Table I for the 20-mm cannon were taken from Reference 1.

The brakes have 4, 8, and 12 rows, respectively, of uniform diameter holes with D = L. The eight-row pattern is shown in Figure 5. The 20-mm brake dimensions were one-sixth those of the 120-mm designs.

In Figure 8, brake efficiency is plotted as a function of the vent area ratio, AR, which is defined as the ratio of the vented area to the bore area. The solid curve labeled L/D = 1 represents the calculated 20-mm data; the three triangular symbols are the 120-mm results. Even though the internal ballistics differs considerably for the two cannons, geometric similarity appears to be sufficient to guarantee nearly the same gasdynamic performance.

The solid curve labeled L/D = 2 represents 20-mm calculations where the wall thickness, L, was doubled but the number of holes was kept the same. This

conforms to the experimental configurations of Reference 1 and facilitates comparison with those data. The asterisk symbol is a 120-mm calculation with L fixed, but D halved to obtain L/D = 2; the number of holes was quadrupled to maintain the area ratio. This is most likely how a high aspect ratio (L/D) would occur in practice. The close agreement between the two sets of calculations suggests that even geometrical similarity is not a strict requirement, rather, the aspect and area ratios may be the controlling parameters. This notion is reinforced by the remaining four symbols on the plot. These represent a portion of the 20-mm experimental data of Reference 1 and correspond to brakes which had only 9 columns of holes and 16, 19, and 23 rows, respectively, rather than 12-row designs studied here.

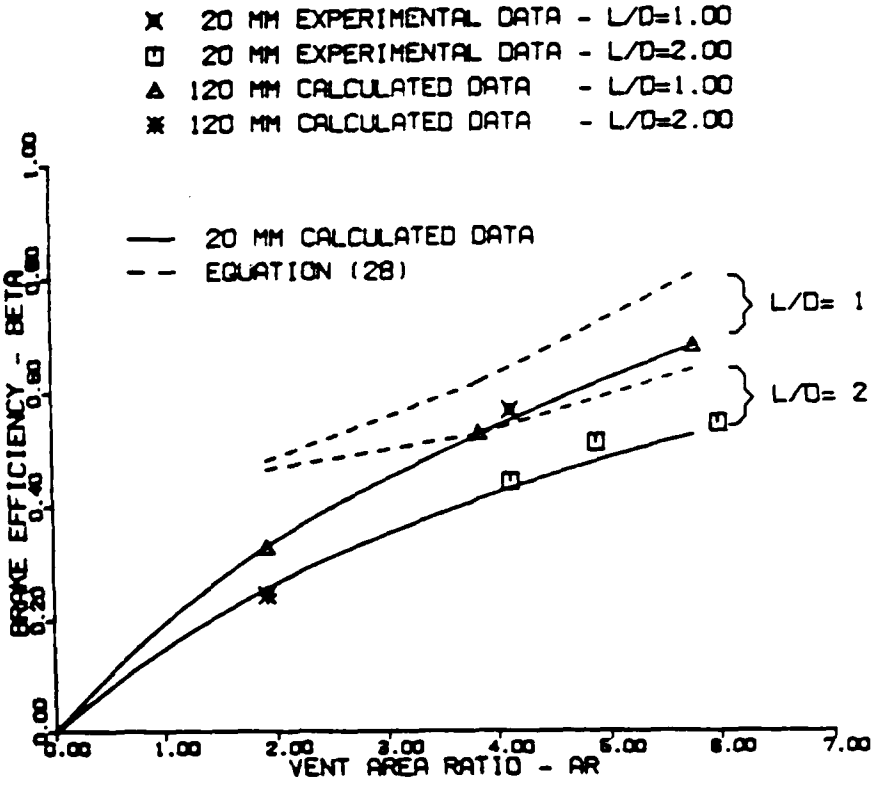


Figure 8. Brake efficiency as a function of vent area ratio, AR.

Dillon (ref 2) recognized the relevance of these two parameters and presented the following formula for brake efficiency:

$$\beta = 0.208 + 0.312(AR) - 0.145(L/D) - 0.062(AR)^2$$
$$+ 0.087(L/D)^2 - 0.039(AR)(L/D) + 0.006(AR)^3 - 0.008(L/D)^3 \qquad (28)$$

The dashed lines in Figure 8 were obtained using this expression. It overestimates the experimental data and the present calculations, particularly at small area ratios. This happens because the formula was based upon a larger sample of brake configurations, some of which were quite different geometrically from the rest.

For example, one brake consisted simply of two holes drilled perpendicular to the bore axis with diameters equal to the bore diameter. While this baffle-like configuration represented an interesting comparison for the more "conventional" perforated brakes, its inclusion in the formula accounts for the two dashed lines converging to a high $\beta$ at AR = 2 in the plot.

Another configuration had vents only on the sides of the tube. The lateral venting arrangement was an attempt to reduce possible obscuration effects associated with axisymmetric venting. As noted in the Introduction, full-scale testing of the idea resulted in damage to finned projectiles. It did produce somewhat higher efficiencies in the 20-mm tests, however, and this contributes to the high estimates of the formula.

Nevertheless, Dillon's idea of possibly representing a wide range of perforated configurations with a single formula has obvious appeal and can be more successfully realized if it is limited to axisymmetric configurations. The curve in Figure 9 represents the formula

$$\beta/(1-0.18\ L/D) = 0.273(AR)[1 - 0.14(AR) + 0.01(AR)^2] \qquad (29)$$

This was obtained using the 20-mm calculations of Figure 8. All of the data in Reference 1 for axisymmetric configurations with aspect ratios between 1 and 2 are shown as well as the uniform and stepped 120-mm data calculated here. This information is summarized in Tables II and III.

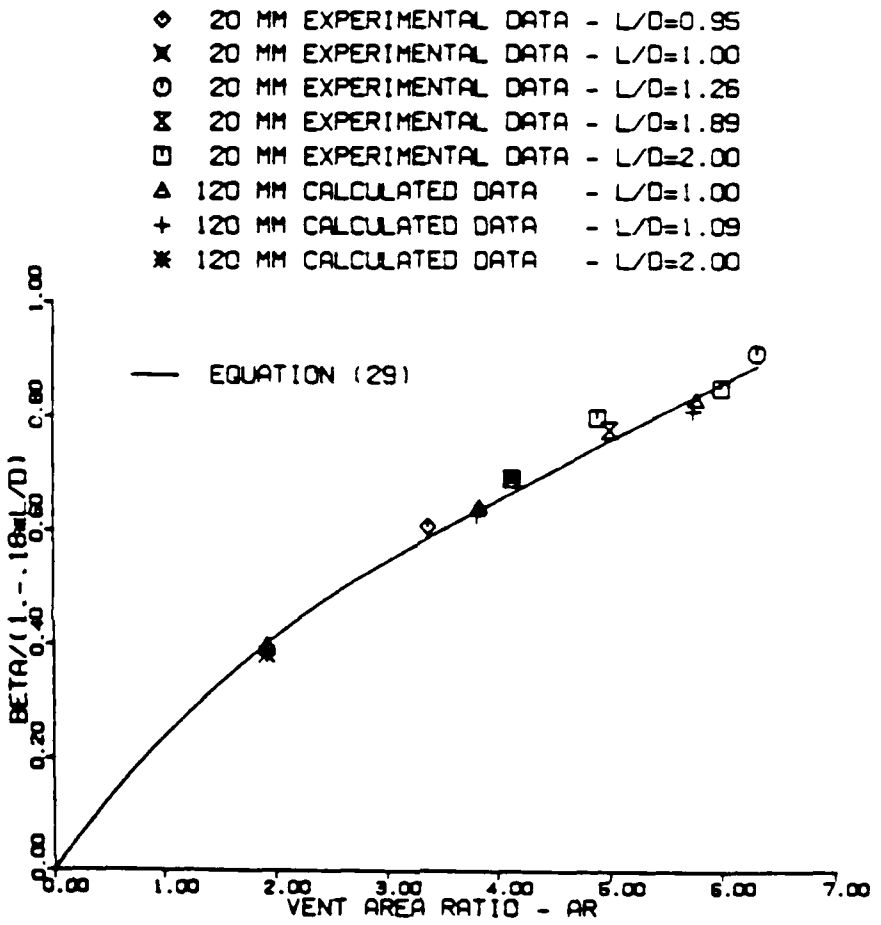


Figure 9. Correlation of computed and experimental brake efficiencies.

The model numbers in Table II correspond to those in Reference 1. However, the values of $\beta$ are slightly lower than reported there. In computing the brake efficiency from the impulse measurements, Dillon used the muzzle velocity obtained with the brake in place rather than the bare muzzle velocity. To be consistent when comparing the various brake configurations, the latter was used here.

TABLE II. SUMMARY OF EXPERIMENTAL DATA FROM REFERENCE 1

| Model | Pattern | AR | L/D | β (%) |
|---|---|---|---|---|
| 1 | staggered | 6.32 | 1.26 | 70.4 |
| 2 | staggered | 5.00 | 1.89 | 51.3 |
| 3 | uniform | 4.13 | 1.00 | 56.8 |
| 4 | uniform | 4.13 | 2.00 | 44.3 |
| 6 | uniform | 4.89 | 2.00 | 51.1 |
| 7 | uniform | 5.99 | 2.00 | 54.4 |
| 8 | staggered & stepped | 3.38 | 0.95 | 50.4 |

TABLE III. SUMMARY OF 120-mm CALCULATIONS

| Model | Pattern | AR | L/D | β (%) |
|---|---|---|---|---|
| A | uniform | 1.92 | 1.00 | 32.8 |
| B | uniform | 3.84 | 1.00 | 52.6 |
| C | uniform | 5.76 | 1.00 | 67.9 |
| D | stepped | 3.82 | 1.09 | 50.5 |
| E | stepped | 5.74 | 1.09 | 65.0 |
| F | uniform | 1.92 | 2.00 | 24.6 |

The staggered patterns in Table II had every other row of 12 holes rotated 15 degrees with respect to the adjacent rows. The uniform pattern refers to the column arrangement shown in Figure 5. Staggering is expected to reduce azimuthal pressure gradients near projectile fins. It does not appear to affect gasdynamic performance, but calculations show that the column pattern produces somewhat lower stresses for a given load (ref 14).

The stepped pattern in Table II had three rows of holes with 1/16-inch diameters, three rows with 1/8-inch diameters, and four rows with 3/16-inch diameters. The center-to-center spacing in the axial direction was constant, as in the stepped pattern of Figure 5, although the rows were staggered. Each row had 12 holes.

To calculate an average hole diameter for the stepped patterns, the following formula was used:

$$\bar{D} = \sum_{n=1}^{N} N_n D_n A_n \Big/ \sum_{n=1}^{N} N_n A_n \qquad (30)$$

where N is the number of different hole sizes and $N_n$ is the number of rows with diameter $D_n$ and area $A_n$. Each diameter is weighted by its area in the belief that a large hole contributes more to brake performance than a small hole. The weighting factor shifts the data closer to the curve in Figure 9.

The close correlation of the tabulated data by the predicted curve supports Dillon's observation that brake performance is primarily dependent on vent area ratio and aspect ratio. Stepped patterns are included by using a suitably weighted average diameter to compute the aspect ratio.

## CONCLUSIONS

The influence on brake performance of including covolume in the three-dimensional calculations was found to be too small to warrant the added computation. The covolume term should be included in the one-dimensional code, however, to be consistent with the internal ballistics code used to generate the starting solution.

Redistributing a given vent area along the tube using a set of holes with varying diameters can result in a structurally more acceptable design with only a modest loss in gasdynamic performance. It may also present a more favorable environment for finned projectiles by reducing axial and azimuthal pressure gradients in the vented portion of the tube.

Brake performance is primarily dependent on vent area ratio and aspect ratio. The dependence can be expressed by a simple formula for axisymmetric designs. Stepped patterns are included by using a suitably weighted average diameter to compute the aspect ratio.

## REFERENCES


1. Dillon, R. E. Jr., "A Parametric Study of Perforated Muzzle Brakes," ARDC Technical Report ARLCB-TR-84015, Benet Weapons Laboratory, Watervliet, NY, May 1984.

2. Dillon, R. E. Jr. and Nagamatsu, H. T., "An Experimental Study of Perforated Muzzle Brakes," ARDC Technical Report ARLCB-TR-84004, Benet Weapons Laboratory, Watervliet, NY, February 1984.

3. Dillon, R. E. Jr. and Nagamatsu, H. T., "A Method of Analyzing Perforated Muzzle Brake Performance," ARDC Technical Report ARLCB-TR-84002, Benet Weapons Laboratory, Watervliet, NY, February 1984.

4. Dillon, R. E. Jr., "Wall Thickness and Vent Area Effects on Perforated Muzzle Brake Performance," ARDC Technical Report ARLCB-TR-84020, Benet Weapons Laboratory, Watervliet, NY, May 1984.

5. Dillon, R. E. Jr. and Nagamatsu, H. T., "An Experimental Study of Perforated Muzzle Brakes," AIAA Paper 84-1642, presented at the AIAA 17th Fluid Dynamics, Plasma Dynamics, and Lasers Conference, June 25-27, 1984, Snowmass, Colorado.

6. Nagamatsu, H. T., Choi, K. Y., Duffy, R. E., and Carofano, G. C., "An Experimental and Numerical Study of the Flow Through a Vent Hole in a Perforated Muzzle Brake," ARDEC Technical Report ARCCB-TR-87016, Benet Weapons Laboratory, Watervliet, NY, June 1987.

7. Nagamatsu, H. T., Choi, K. Y., and Duffy, R. E., "Wall Thickness and Flow Mach Number Effects on Pressure Distribution in the Vent Hole for Perforated Muzzle Brakes," ARDEC Contractor Report ARCCB-CR-86038, Rensselaer Polytechnic Institute, Troy, NY, November 1986.

8. Corner, J., Theory of the Interior Ballistics of Guns, John Wiley and Sons, New York, 1950.

9. Fansler, K. S., "A Simple Method for Predicting Muzzle Brake Effectiveness and Baffle-Surface Pressure," Technical Report ARBRL-TR-02335, Ballistic Research Laboratory, Aberdeen Proving Ground, Maryland, June 1981.

10. Pater, L. L., "Scaling of Muzzle Brake Performance and Blast Field," Technical Report TR-3049, Naval Surface Weapons Center, Dahlgren Laboratory, Dalhgren, Virginia, October 1974.

11. Pater, L. L., "Muzzle Brake Parameter Study," Technical Report TR-3531, Naval Surface Weapons Center, Dahlgren Laboratory, Dalhgren, Virginia, October 1976.

12. Harten, A., "High Resolution Schemes for Hyperbolic Conservation Laws," J. Computational Physics, Vol. 49, No. 3, March 1983, pp. 357-393.

13. Zucrow, M. J. and Hoffman, J. D., Gas Dynamics - Volume 2: Multidimensional Flow, John Wiley and Sons, New York, 1977, Chapter 19.

14. Glennon, M., Private Communication, US Army ARDEC, Benet Weapons Laboratory, Watervliet, NY, February 1987.

TECHNICAL REPORT INTERNAL DISTRIBUTION LIST

| | NO. OF COPIES |
|---|---|
| CHIEF, DEVELOPMENT ENGINEERING BRANCH | |
| ATTN: SMCAR-CCB-D | 1 |
| -DA | 1 |
| -DC | 1 |
| -DM | 1 |
| -DP | 1 |
| -DR | 1 |
| -DS (SYSTEMS) | 1 |
| CHIEF, ENGINEERING SUPPORT BRANCH | |
| ATTN: SMCAR-CCB-S | 1 |
| -SE | 1 |
| CHIEF, RESEARCH BRANCH | |
| ATTN: SMCAR-CCB-R | 2 |
| -R (ELLEN FOGARTY) | 1 |
| -RA | 1 |
| -RM | 1 |
| -RP | 1 |
| -RT | 1 |
| TECHNICAL LIBRARY<br>ATTN: SMCAR-CCB-TL | 5 |
| TECHNICAL PUBLICATIONS & EDITING UNIT<br>ATTN: SMCAR-CCB-TL | 2 |
| DIRECTOR, OPERATIONS DIRECTORATE<br>ATTN: SMCWV-OD | 1 |
| DIRECTOR, PROCUREMENT DIRECTORATE<br>ATTN: SMCWV-PP | 1 |
| DIRECTOR, PRODUCT ASSURANCE DIRECTORATE<br>ATTN: SMCWV-QA | 1 |

NOTE: PLEASE NOTIFY DIRECTOR, BENET LABORATORIES, ATTN: SMCAR-CCB-TL, OF ANY ADDRESS CHANGES.

TECHNICAL REPORT EXTERNAL DISTRIBUTION LIST

| | NO. OF COPIES |
|---|---|
| ASST SEC OF THE ARMY<br>RESEARCH AND DEVELOPMENT<br>ATTN: DEPT FOR SCI AND TECH<br>THE PENTAGON<br>WASHINGTON, D.C. 20310-0103 | 1 |
| ADMINISTRATOR<br>DEFENSE TECHNICAL INFO CENTER<br>ATTN: DTIC-FDAC<br>CAMERON STATION<br>ALEXANDRIA, VA 22304-6145 | 12 |
| COMMANDER<br>US ARMY ARDEC<br>ATTN: SMCAR-AEE | 1 |
| SMCAR-AES, BLDG. 321 | 1 |
| SMCAR-AET-O, BLDG. 351N | 1 |
| SMCAR-CC | 1 |
| SMCAR-CCP-A | 1 |
| SMCAR-FSA | 1 |
| SMCAR-FSM-E | 1 |
| SMCAR-FSS-D, BLDG. 94 | 1 |
| SMCAR-MSI (STINFO)<br>PICATINNY ARSENAL, NJ 07806-5000 | 2 |
| DIRECTOR<br>US ARMY BALLISTIC RESEARCH LABORATORY<br>ATTN: SLCBR-DD-T, BLDG. 305<br>ABERDEEN PROVING GROUND, MD 21005-5066 | 1 |
| DIRECTOR<br>US ARMY MATERIEL SYSTEMS ANALYSIS ACTV<br>ATTN: AMXSY-MP<br>ABERDEEN PROVING GROUND, MD 21005-5071 | 1 |
| COMMANDER<br>HQ, AMCCOM<br>ATTN: AMSMC-IMP-L<br>ROCK ISLAND, IL 61299-6000 | 1 |
| COMMANDER<br>ROCK ISLAND ARSENAL<br>ATTN: SMCRI-ENM<br>ROCK ISLAND, IL 61299-5000 | 1 |
| DIRECTOR<br>US ARMY INDUSTRIAL BASE ENGR ACTV<br>ATTN: AMXIB-P<br>ROCK ISLAND, IL 61299-7260 | 1 |
| COMMANDER<br>US ARMY TANK-AUTMV R&D COMMAND<br>ATTN: AMSTA-DDL (TECH LIB)<br>WARREN, MI 48397-5000 | 1 |
| COMMANDER<br>US MILITARY ACADEMY<br>ATTN: DEPARTMENT OF MECHANICS<br>WEST POINT, NY 10996-1792 | 1 |
| US ARMY MISSILE COMMAND<br>REDSTONE SCIENTIFIC INFO CTR<br>ATTN: DOCUMENTS SECT, BLDG. 4484<br>REDSTONE ARSENAL, AL 35898-5241 | 2 |
| COMMANDER<br>US ARMY FGN SCIENCE AND TECH CTR<br>ATTN: DRXST-SD<br>220 7TH STREET, N.E.<br>CHARLOTTESVILLE, VA 22901 | 1 |
| COMMANDER<br>US ARMY LABCOM<br>MATERIALS TECHNOLOGY LAB<br>ATTN: SLCMT-IML (TECH LIB)<br>WATERTOWN, MA 02172-0001 | 2 |

NOTE: PLEASE NOTIFY COMMANDER, ARMAMENT RESEARCH, DEVELOPMENT, AND ENGINEERING CENTER, US ARMY AMCCOM, ATTN: BENET LABORATORIES, SMCAR-CCB-TL, WATERVLIET, NY 12189-4050, OF ANY ADDRESS CHANGES.

TECHNICAL REPORT EXTERNAL DISTRIBUTION LIST (CONT'D)

| | NO. OF COPIES |
|---|---|
| COMMANDER<br>US ARMY LABCOM, ISA<br>ATTN: SLCIS-IM-TL<br>2800 POWDER MILL ROAD<br>ADELPHI, MD 20783-1145 | 1 |
| COMMANDER<br>US ARMY RESEARCH OFFICE<br>ATTN: CHIEF, IPO<br>P.O. BOX 12211<br>RESEARCH TRIANGLE PARK, NC 27709-2211 | 1 |
| DIRECTOR<br>US NAVAL RESEARCH LAB<br>ATTN: MATERIALS SCI & TECH DIVISION<br>CODE 26-27 (DOC LIB)<br>WASHINGTON, D.C. 20375 | 1<br>1 |
| COMMANDER<br>AIR FORCE ARMAMENT LABORATORY<br>ATTN: AFATL/MN<br>EGLIN AFB, FL 32542-5434 | 1 |
| COMMANDER<br>AIR FORCE ARMAMENT LABORATORY<br>ATTN: AFATL/MNF<br>EGLIN AFB, FL 32542-5434 | 1 |
| METALS AND CERAMICS INFO CTR<br>BATTELLE COLUMBUS DIVISION<br>505 KING AVENUE<br>COLUMBUS, OH 43201-2693 | 1 |

NOTE: PLEASE NOTIFY COMMANDER, ARMAMENT RESEARCH, DEVELOPMENT, AND ENGINEERING CENTER, US ARMY AMCCOM, ATTN: BENET LABORATORIES, SMCAR-CCB-TL, WATERVLIET, NY 12189-4050, OF ANY ADDRESS CHANGES.